Wavelet approximation coupled with fictitious domain approach. Applications to the Stefan problem *

BACCOU JEAN

IRSN and LATP, Technopôle de Château-Gombert, 13451 Marseille Cedex 20, France

jean.baccou@irsn.fr

CHIAVASSA GUILLAUME

MN2MP and Centrale Marseille, Technopôle de Château-Gombert, 13451 Marseille Cedex 20, France

guillaume.chiavassa@ec-marseille.fr

KOZUBEK THOMAS

Dept of applied Mathematics, VSB-Technical University of Ostrava, 70833 Ostrava, Czech republik

tomas.kozubek@vsb.cz

LIANDRAT JACQUES

LATP and Centrale Marseille, Technopôle de Château-Gombert, 13451 Marseille Cedex 20, France

jacques.liandrat@ec-marseille.fr

Received (Day Month Year)
Revised (Day Month Year)
Communicated by (xxxxxxxxxx)

Abstract:

The paper starts with a refined analysis of a method recently developed, based on wavelet-fictitious domain solver for the 2D heat equation on general domains (^{2}). Special attention is devoted to the analysis of the approximation of the solution and its normal gradient at the boundary of the domain. This analysis leads to embed the method in a more general formulation for the approximation of Stefan like problems where it is known that the approximation at the boundary of the domain is crucial. Coupling the original method with an adapted level set approach provides a new method for the numerical resolution of such problems. This method is tested on various examples.

Keywords: Stefan problem, wavelets, fictitious domain, level set method

*Research partially supported by European network "Breaking Complexity" #HPRN-CT-2002-00286

1. Introduction

Wavelet numerical methods have been widely developed in the last decade for partial differential equations raised on simple domains (for instance see [11]). For complex domains, few approaches have been more recently investigated, including domain decomposition ([6]), penalization methods ([28]) and Lagrange multiplier methods ([17]).

In a recent paper ([2]), a new method coupling wavelet approximations and the Lagrange multipliers fictitious domain approach ([15]) has been presented. This method has been analyzed and first results on its stability and efficiency have been established. The main results of ([2]) are the following:

First, diagonal preconditioners in wavelet bases are available to stabilize and speed up the method; low complexity algorithms can then be defined in the framework of tensorial products of periodized spline multi-resolution. Second, a global error estimate has been established. It is connected to the global regularity of the solution on the fictitious domain. It is known that, as soon as the multipliers are non zero, the solution globally belongs to $H^{\frac{3}{2}-\epsilon}$, $\epsilon > 0$. Therefore, the global error estimate lead to a slow convergence towards the solution.

In this paper, we first aim to refine the investigation of the advantages of the use of wavelets in the proposed framework (Section 2). We start by focussing on the approximation of the solution on the whole domain and show that adaptive spaces of approximation can circumvent the low convergence rate of the error. Then, we show, following ([4]) that an optimal convergence rate on any interior domain is available. The approximation of Lagrange multipliers that appear in the method is finally investigated. We establish an error estimate for the normal derivative jump of the solution along the boundary that emphasizes the advantage of using high order approximation spaces of wavelet type for Lagrange multipliers also.

All these results lead to the fact that the wavelet/fictitious domain approach can be used in the framework of Stefan problem ([29]) simulations.

In the second part of the paper (starting from Section 3), we therefore focus on the definition and the implementation of a wavelet fictitious domain approach coupled with a level set method for the numerical resolution of the Stefan problem. Here, a simple version of this problem is formulated as a classical initial value problem for a parabolic differential equation on a domain for which a portion of the boundary (the free boundary) is a priori unknown and therefore requires to solve a coupled auxiliary equation. At each time, a new domain is used. The time evolution of the domain relies on the estimate of the solution of the parabolic equation on the domain and of course on the solution of the free boundary equation. Therefore, such a problem is a very good test to illustrate the efficiency of the newly developed wavelet method. Up to our knowledge, wavelet methods have never been used in such a context.

The literature on the Stefan problem and its approximation is very large and we refer to the following books, lectures, articles and references therein for the description of the main results on the subject ([19], [1], [24], [23]).

From the introduction of the continuous Stefan problem and its reformulation using the level set formalism (Section 3), the paper is organized as follows: Section 4 is devoted to the description of the different steps of discretization while the numerical implementation is presented in Section 5. Numerical results on various examples are provided in Section 6.

2. Wavelet approximation coupled to the fictitious domain approach

After a short review of the approach proposed in [2] we derive successively theoretical and numerical estimates for errors related to global approximation, interior approximation and normal gradient jump approximation. These quantities, that will be precisely defined later on, are known to be key variables in the simulation of Stefan-like problems.

2.1. *An overview of the approach*

Given an open set $\omega \in I\!R^2$ of boundary γ , $T > 0$, $f \in C^0([0,T], C^0(\omega))$ and $g \in C^0([0,T], C^0(\gamma))$ where C^0 stands for the space of continuous functions, we consider the following problem in the strong formulation:

$$\begin{cases} \text{Find } u \text{ such that} \\ \frac{\partial u}{\partial t} + Lu = f \text{ in } \omega \times [0,T], \\ u|_\gamma = g \text{ on } \gamma, \\ u(t=0,.) = u_0 \text{ in } \omega. \end{cases} \tag{2.1}$$

It is first discretized in time using a finite difference scheme associated to a segmentation $t_0 = 0 < t_1 < ... < t_n < ... < t_M = T$ of $[0,T]$ with $\delta t_n = t_{n+1} - t_n$. If u^n stands for the approximation of $u(t_n, x)$, the time semi- discretized problem, reads, for a single step finite difference scheme

$$\forall n \in [0, M-1] \quad \begin{cases} \text{Find } u^{n+1} \text{ such that} \\ L_1 u^{n+1} = L_2 u^n + f^n \text{ in } \omega, \\ u^{n+1}|_\gamma = g^{n+1} \text{ on } \gamma, \\ u^0 = u_0 \text{ in } \omega, \end{cases} \tag{2.2}$$

where L_1 and L_2 are finite difference operators, $f^n = f(t_n, .)$ and $g^{n+1} = g(t_{n+1}, .)$.
At each time t_n, assuming that u^n is known, formulation (2.2) is an elliptic problem raised in ω with Dirichlet conditions on γ.
Following Ref. [16], the fictitious domain approach with Lagrange multipliers on γ transforms (2.2) into a saddle point problem of the form

$$\forall n \in [0, M-1] \quad \begin{cases} \text{Find } U^{n+1} \in H(\Omega) \text{ and } \lambda^{n+1} \in G(\gamma) \text{ such that} \\ a_\Omega(U^{n+1}, V) - \nu\delta t b(V, \lambda^{n+1}) = l_{\Omega,n}(V) \quad \forall V \in H(\Omega), \\ b(U^{n+1}, \mu) =< g^{n+1}, \mu >_\gamma \quad \forall \mu \in G(\gamma), \\ U^0 = U_0 \quad \text{in } \Omega. \end{cases} \tag{2.3}$$

The solution U^n is now defined on a domain Ω in which ω is embedded (see Figure 1) and $H(\Omega)$ as well as $G(\gamma)$ are suitable functional spaces. Moreover, $< , >_\gamma$ stands for the duality pairing between $G(\gamma)$ and its dual.

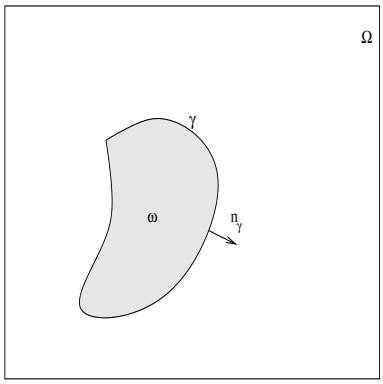

Fig. 1. Domains and boundaries

Introducing multi-resolution approximations of $H(\Omega)$ (resp. of $G(\gamma)$), the full discretization of (2.3) is performed substituting finite dimension spaces to $H(\Omega)$ (resp $G(\gamma)$) in (2.3).

To continue the description of the approach, we fix $\Omega = [a, b]^2$, $L = -\nu\Delta$ where $\nu > 0$ and Δ stands for the Laplacian operator. Taking the implicit Euler scheme for a constant time discretization step, δt, we have $L_1 = (Id - \nu\delta t\Delta)$ and $L_2 = Id$, where Id is the identity operator. Then, $H(\Omega) = H^1_{\mathcal{P}}(\Omega)$, the sub- space of $H^1(\Omega)$ of periodic functions.

a_Ω and $l_{\Omega,n}$ are given by,

$$a_\Omega \begin{cases} H^1_{\mathcal{P}}(\Omega) \times H^1_{\mathcal{P}}(\Omega) \to I\!R \\ (U, V) \mapsto \int_\Omega (\nu\delta t \nabla U \nabla V + UV) \; dxdy, \end{cases} \tag{2.4}$$

and

$$l_{\Omega,n} \begin{cases} H^1_{\mathcal{P}}(\Omega) \to I\!R \\ V \mapsto \int_\Omega U^n V \; dxdy. \end{cases} \tag{2.5}$$

It is useful for the rest of this work to introduce R_ω, resp. $R_{\Omega\backslash\bar{\omega}}$, the restriction operator from $H^1_{\mathcal{P}}(\Omega)$ to $H^1(\omega)$, resp. to $H^1(\Omega\backslash\bar{\omega})$. We assume that R_ω and $R_{\Omega\backslash\bar{\omega}}$ are bounded linear operators such that $\forall u \in H^1_{\mathcal{P}}(\Omega)$, $|| u ||^2_{H^1(\Omega)} = || R_\omega u ||^2_{H^1(\omega)} + || R_{\Omega\backslash\bar{\omega}} u ||^2_{H^1(\Omega\backslash\bar{\omega})}$.
Using this restriction operator, the bilinear form b reads,

$$b \begin{cases} H^1_{\mathcal{P}}(\Omega) \times H^{-1/2}(\gamma) \to I\!R \\ (V, \mu) \mapsto < \gamma_0 \left(R_\omega V\right), \mu >_\gamma, \end{cases} \tag{2.6}$$

with γ_0 the first trace application from $H^1(\omega)$ to $H^{1/2}(\gamma)$.

Existence and uniqueness of the solution of (2.3) is classically ensured ([5], [16]) and $\forall n$, $R_\omega U^n = u^n$. The main ingredients to prove existence and uniqueness is the ellipticity and continuity of the bilinear form, a_Ω, and the Inf-Sup condition satisfied by b. These three conditions read: $\exists K, \xi, \beta$ such that

$$| a_\Omega(U, V) | \leq K || U ||_{H^1(\Omega)} || V ||_{H^1(\Omega)}, \ \forall U \in H^1(\Omega), \ \forall V \in H^1(\Omega), \tag{2.7}$$

$$\sup_{V \in H^1(\Omega), V \neq 0} \frac{a_\Omega(U, V)}{|| V ||_{H^1(\Omega)}} \geq \xi || U ||_{H^1(\Omega)}, \ \forall U \in H^1(\Omega), \tag{2.8}$$

$$\sup_{U \in H^1(\Omega)} a_\Omega(U, V) > 0, \ \forall V \in H^1(\Omega), \ V \neq 0, \tag{2.9}$$

$$\sup_{V \in H^1(\Omega), V \neq 0} \frac{b(V, \mu)}{|| V ||_{H^1(\Omega)}} \geq \beta || \mu ||_{H^{-1/2}(\gamma)}, \ \forall \mu \in H^{-1/2}(\gamma). \tag{2.10}$$

To perform the full discretization, we choose a Petrov-Galerkin method and therefore introduce three finite dimensional subspaces $U^\Omega_h \subset H^1_{\mathcal{P}}(\Omega)$, $V^\Omega_h \subset H^1_{\mathcal{P}}(\Omega)$ and $Q^\gamma_{h'} \subset H^{-1/2}(\gamma)$.
For every $n \geq 0$, System (2.3) is then replaced by

$$\begin{cases} \text{Find } \left(U^{n+1}_h, \lambda^{n+1}_{h'}\right) \in U^\Omega_h \times Q^\gamma_{h'}, \text{ such that} \\ a_\Omega(U^{n+1}_h, V_h) - \nu\delta t b(V_h, \lambda^{n+1}_{h'}) = l_{\Omega,n,h}(V_h) \ \ \forall V_h \in V^\Omega_h, \\ b(U^{n+1}_h, \mu_{h'}) = < g^{n+1}, \mu_{h'} >_\gamma \quad \forall \mu_{h'} \in Q^\gamma_{h'}, \end{cases} \tag{2.11}$$

where $l_{\Omega,n,h}$ is obtained replacing U^n by U^n_h in $l_{\Omega,n}$.

Assuming $V^\Omega_h \subset H^2_{\mathcal{P}}(\Omega)$ and using Green formulas, it can be rewritten for every $n \geq 0$ as

$$\begin{cases} \text{Find } \left(U_h^{n+1}, \lambda_{h'}^{n+1}\right) \in U_h^\Omega \times Q_{h'}^\gamma, \text{ such that} \\ \\ \int_\Omega U_h^{n+1}(V_h - \nu\delta t \Delta V_h)\, dxdy - \nu\delta t b(V_h, \lambda_{h'}^{n+1}) = \int_\Omega U_h^n V_h\, dxdy \ \forall V_h \in V_h^\Omega, \\ b(U_h^{n+1}, \mu_{h'}) =< g^{n+1}, \mu_{h'} >_\gamma \quad \forall \mu_{h'} \in Q_{h'}^\gamma. \end{cases} \tag{2.12}$$

We take for U_h^Ω the spaces $\left\{U_j^\Omega\right\}_{j\in\mathbb{Z}}$ of an orthogonal m-regular [a] multi-resolution of $H^1_{\mathcal{P}}(\Omega)$ with $h = 2^{-j}$ (see Ref. [20]). In numerical tests, we choose the periodized splines of order m related to regular dyadic points. Following Ref. [9] and assuming $m > 2$, we choose for V_h^Ω the image of U_j^Ω by the operator $(I - \nu\delta t\Delta)^{-1}$, i.e $\forall j \in \mathbb{Z}$, $V_j^\Omega = (I - \nu\delta t\Delta)^{-1} U_j^\Omega$. Such spaces are generated by Bi-orthogonal "vaguelettes" (Ref. [20]) and inherit the essential properties of classical multi-resolution spaces.
Similarly, we take for $Q_{h'}^\gamma$ the spaces $\{Q_{j'}^\gamma\}_{j'\in\mathbb{Z}}$ of an orthogonal multi-resolution of $H^{-1/2}(\gamma)$ of regularity $m' \geq 1$ with $h' = 2^{-j'}$. Assuming that γ is a boundary of regularity C^1, such a multi-resolution can be constructed transporting on γ a multi-resolution of $H^{-1/2}(]0,1[)$ (Ref. [12]).
For the sake of completeness, we specify the following classical notations and definitions.

For every $j \in \mathbb{N}$, we note $K_j = \left\{\alpha = (j, k_1, k_2), k_1 = 0, ..., 2^j - 1;\ k_2 = 0, ..., 2^j - 1\right\}$ with $|\alpha| = j$ and $K_{-1} = \{(-1, 0, 0)\}$; we also introduce $A_j = K_j \times \{1, 2, 3\}$ and $A_{-1} = K_{-1} \times \{1\}$. We then have,

Definition 2.1.
The two approximation spaces U_j^Ω and V_j^Ω are constructed as follows:
- $U_j^\Omega = span\left\{\phi_\alpha^\Omega, \alpha \in K_j\right\} = span\left\{\psi_\alpha^{\Omega,i}, (\alpha, i) \in A_l,\ -1 \leq l \leq j-1\right\}$ with $\psi_\alpha^{\Omega,i} = \phi_0^\Omega$ if $(\alpha, i) \in A_{-1}$ and ϕ_α^Ω (resp. $\psi_\alpha^{\Omega,i}$, $i \in \{1, 2, 3\}$) the scaling functions (resp. the wavelets) of a m-regular multi-resolution analysis.
- $V_j^\Omega = span\left\{\theta_\alpha^{\Omega,i},\ (\alpha, i) \in A_l,\ -1 \leq l \leq j-1\right\}$ with $\forall (\alpha, i) \in A_l,\ l \geq 0,\ \theta_\alpha^{\Omega,i} = (I - \nu\delta t\Delta)^{-1} \psi_\alpha^{\Omega,i}$ and $\theta_\alpha^{\Omega,i} = (I - \nu\delta t\Delta)^{-1} \phi_0^\Omega$ if $(\alpha, i) \in A_{-1}$.
Note that, due to the periodic boundary conditions, the functions $\theta_\alpha^{\Omega,i}$ are indeed well defined. The functions $\theta_\alpha^{\Omega,i}$ share the classical localization properties of wavelets. Moreover, introducing $\tilde{\theta}_\alpha^{\Omega,i} = (I - \nu\delta t\Delta)\, \psi_\alpha^{\Omega,i}$, we obtain $\forall(\alpha_1, \alpha_2)$ and $\forall(i_1, i_2)$, $< \theta_{\alpha_1}^{\Omega,i_1}, \tilde{\theta}_{\alpha_2}^{\Omega,i_2} >_{L^2(\Omega)} = \delta_{\alpha_1,\alpha_2}\delta_{i_1,i_2}$. The two families $\{\theta_\alpha^{\Omega,i}\}_{\alpha,i}$ and $\{\tilde{\theta}_\alpha^{\Omega,i}\}_{\alpha,i}$ are therefore called bi-orthogonal "vaguelettes" (Ref. [20]).

In [2], an existence and uniqueness theorem for Problem (2.12) with the approximation spaces of Definition 2.1 has been proved and the related numerical

[a] if ϕ is the scaling function of a multi-resolution analysis, the m-regularity property reads: ϕ is differentiable up to order m, $\phi \in C^{m-1}$ and $\forall(\alpha_1, \alpha_2)$ with $\alpha_1 + \alpha_2 \leq m$, $\forall r$, $\exists c_r$, such that $|\frac{\partial^{\alpha_1+\alpha_2}}{\partial x^{\alpha_1}\partial y^{\alpha_2}}\phi| \leq \frac{c_r}{\left(1+\sqrt{x^2+y^2}\right)^r}$

implementation has been presented. It comes out that diagonal preconditioners are available for the stabilization of the iterative procedures related to (2.12). Here, we focus on the quality of the approximation and therefore investigate different approximation errors.

2.2. *Global approximation error*

The following global approximation error has been proved in [2]:

Proposition 2.1.
Let u (resp U_h^n) be the unique solution of problem (2.1) with $L = -\nu\Delta$ (resp of problem (2.11)), then

$$|| u(t_{n+1},.) - R_\omega U_h^{n+1} ||_{L^2(\omega)} \leq || u(t_0,.) - u^0 ||_{L^2(\omega)} + || U_h^0 - U^0 ||_{L^2(\Omega)} + cT\delta t + \frac{c'T}{\delta t}\left(2^{-js} + 2^{-j's'}\right), \quad (2.13)$$

where c and c' are two constants that do not depend on h, h' and δt.

It is known that the value of s in the previous estimate is limited by $3/2$ as soon as the Lagrange multipliers are non zeros since $\forall n,\ \lambda^n = [\frac{\partial U^n}{\partial n_\gamma}]_\gamma$, where $[\frac{\partial .}{\partial n_\gamma}]_\gamma$ stands for the normal gradient jump at the boundary γ. Numerical estimates available on Figure 2 indeed reveal the slope $-3/2$ in the log-log plot of the global error versus the dimension 2^j. For that figure, as well as for the sequel of Section 2, $\omega =]0,1[\times]0,0.5[$, $\Omega =]0,1[^2$, $U_0(x,y) = sin(2\pi y)sin(6\pi x)$ in ω and $U_0(x,y) = -sin(2\pi y)sin(6\pi x)$ in $\Omega\backslash\omega$. Moreover, $g = 0$ and $L(u) = -\frac{1}{40\pi^2}\Delta(u)$.

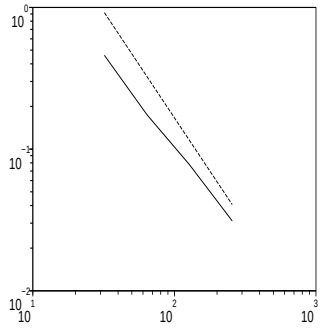

Fig. 2. Global error versus dimension (2^j) (log-log scale). The dash-line stands for the theoretical error bound (slope $-3/2$) whereas the continuous one stands for the numerical estimate

The limitation of s is inherent to the use of Lagrange multipliers since, as soon as $\lambda \neq 0$, the largest possible exponent of global regularity for U is $3/2$. Specific

extension procedures as derived in [21] could be used to enforce $\lambda = 0$ but are not investigated here because they can not be used starting from Section 3. A remedy to the lack of regularity is the adaption of the space of approximation, fighting against local non regularity by local refinement. We show on Figure 3 the L^2 global error plotted versus N for the best N term approximation of U_j^n.

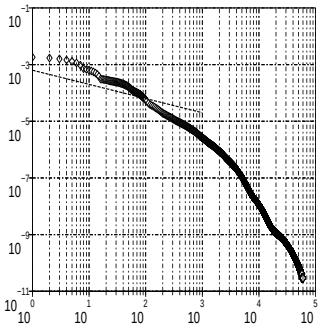

Fig. 3. Global error for the best N term approximation versus N. The dash-line stands for the theoretical decay (slope $-3/2$)

The localization of the biggest coefficients (see Figure 4) clearly shows that a local refinement in the vicinity of γ (in the computation corresponding to the figure $\gamma = \{y = 0\} \bigcup \{y = 0.5\} \bigcup \{y = 1\}$) is efficient to improve the approximation of the solution.

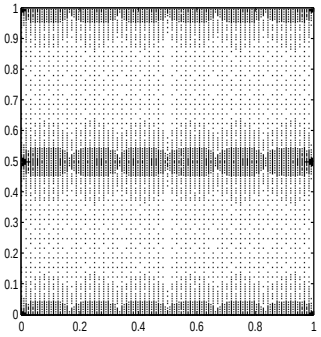

Fig. 4. Localization of the $N = 8035$ biggest coefficients

2.3. *Interior approximation error*

The previous error estimates and associated comments and numerical results put into evidence the limitations on the decay of the error due to the lack of global regularity of the solution. However, it will be shown in this chapter that the approximation is optimal on any open sub-domain $\omega_0 \subset \omega$ with $\bar{\omega_0} \bigcap \gamma = \emptyset$.

For some Galerkin methods, according to J. Nitsche and A. Schatz ([22]) and specifically for standard wavelet Galerkin methods based on compactly supported bi-orthogonal wavelet bases, S. Bertoluzza in ([4]) has established that

Proposition 2.2.
If u is the solution of the following problem:

$$\int_\omega \nabla u \nabla v + \int_\omega uv = \int_\omega fv + \int_\gamma gv, \ \forall v \in H^1(\omega), \tag{2.14}$$

and if u_h is the approximation of u in V_h a wavelet-spanned approximation space, by means of a Galerkin method, then, for any open set $\omega_0 \subset \omega$ with $\bar{\omega_0} \bigcap \gamma = \emptyset$, there exists an open set ω_1 with $\omega_0 \subset \omega_1 \subset \omega$ such that

$$||u - u_h||_{L^2(\omega_0)} \leq C(2^{-jl}||u||_{H^l(\omega_1)} + ||u - u_h||_{H^{-p}(\omega_1)}), \tag{2.15}$$

with $u \in H^s(\omega_1)$, $l = min(s, r)$ (with r the number of moments of the wavelet) and p a non-negative integer, arbitrary but fixed.

Starting from a more general situation introduced in [22] (allowing a solution-dependent right hand side in the formulation (2.14)), this result can naturally be applied to each elliptic problem of type (2.2) and extended to the case of fictitious domain Galerkin methods. It gives, $\forall n \in [0, M-1]$,

$$\begin{aligned} ||R_{\omega_0}(U^{n+1} - U_h^{n+1})||_{L^2(\omega_0)} \leq C(2^{-jl}||R_{\omega_1}U^{n+1}||_{H^l(\omega_1)} + ||R_{\omega_1}(U^{n+1} - U_h^{n+1})||_{H^{-p}(\omega_1)} \\ + 2^{-j}||R_{\omega_1}(U^n - U_h^n)||_{H^1(\omega_1)} + ||R_{\omega_1}(U^n - U_h^n)||_{L^2(\omega_1)}). \end{aligned} \tag{2.16}$$

Therefore, up to some correcting terms and provided $\bar{\omega}_1 \cap \gamma = \emptyset$, the error estimate in the interior domain ω_0 of ω is optimal.

The adaption of this result to our formulation is not straightforward since on one hand our method is of Petrov-Galerkin type and on the other hand it does not use compactly supported wavelets and vaguelettes. However, we have been able to establish a generalization of (2.16) adapted to this situation, a result that will be published elsewhere ([3]).
Numerical results associated to this estimate are reported on Figure 5 where $\omega_0 =]0.4, 0.6[\times]0, 1[$. One can observe a first decay of the error with a slope $s = -2m = -8$ corresponding to a superconvergence behaviour (see for instance [9])followed by a saturation from $j = 6$.

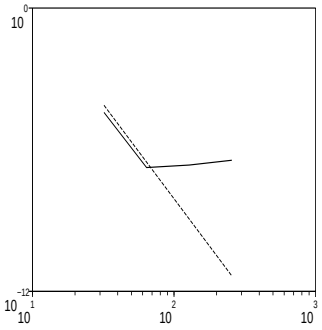

Fig. 5. Local error versus dimension (2^j) (log-log scale). The dash-line stands for the theoretical error bound (slope $-2m = 8$) whereas the continuous one stands for the numerical estimate

2.4. *Error bounds on the normal gradient jump*

According to the previous sections, the gradient of the solution normal to the boundary γ is discontinuous crossing γ as soon as the Lagrange multipliers are non zeros. It turns out to be that in many applications, the normal gradient is a key quantity. In our framework, we have the following estimate related to the normal gradient jump at the boundary:

Theorem 2.1. *Let U^n (resp U_h^n) be the unique solution of problem (2.3) (resp of problem (2.11)), then*

$$|||[\frac{\partial U^{n+1}}{\partial n_\gamma}]_\gamma - [\frac{\partial U_h^{n+1}}{\partial n_\gamma}]_\gamma||_{H^{-1/2}(\gamma)} \leq c\ ||\lambda^n - \lambda_{h'}^n||_{H^{-1/2}(\gamma)} + \frac{c'}{\nu\delta t}\ ||U_h^{n-1} - U^{n-1}||_{L_2(\Omega)},$$

where c and c' are two constants that do not depend on j, j' and δt.

Proof. The goal is to show that $|||[\frac{\partial U^{n+1}}{\partial n_\gamma}]_\gamma - [\frac{\partial U_h^{n+1}}{\partial n_\gamma}]_\gamma||_{H^{-1/2}(\gamma)}$ is controlled by $||\lambda^{n+1} - \lambda_{h'}^{n+1}||_{H^{-1/2}(\gamma)}$ and $||U_h^n - U^n||_{L_2(\Omega)}$.

Let's start by writing,

$$\begin{aligned}|||[\frac{\partial U^{n+1}}{\partial n_\gamma}]_\gamma - [\frac{\partial U_h^{n+1}}{\partial n_\gamma}]_\gamma||_{H^{-1/2}(\gamma)} &= ||(\frac{\partial R_\omega U^{n+1}}{\partial n_\gamma^+} - \frac{\partial R_\omega U_h^{n+1}}{\partial n_\gamma^+}) - (\frac{\partial R_{\Omega\setminus\bar{\omega}} U^{n+1}}{\partial n_\gamma^-} - \frac{\partial R_{\Omega\setminus\bar{\omega}} U_h^{n+1}}{\partial n_\gamma^-})||_{H^{-1/2}(\gamma)},\\ &\leq 2max(||\frac{\partial R_\omega U^{n+1}}{\partial n_\gamma^+} - \frac{\partial R_\omega U_h^{n+1}}{\partial n_\gamma^+}||_{H^{-1/2}(\gamma)}, ||\frac{\partial R_{\Omega\setminus\bar{\omega}} U^{n+1}}{\partial n_\gamma^-} - \frac{\partial R_{\Omega\setminus\bar{\omega}} U_h^{n+1}}{\partial n_\gamma^-}||_{H^{-1/2}(\gamma)}),\end{aligned}$$

where $\frac{\partial\ .}{\partial n_\gamma^+}$ (resp. $\frac{\partial\ .}{\partial n_\gamma^-}$) denotes the derivative following the outer (resp. inner) normal to the boundary γ.

In what follows, we focus on exhibiting a bound for $||\frac{\partial R_\omega U^{n+1}}{\partial n_\gamma^+} - \frac{\partial R_\omega U_h^{n+1}}{\partial n_\gamma^+}||_{H^{-1/2}(\gamma)}$. For the sake of clarity in this proof, we note $u^{n+1} = R_\omega U^{n+1}$ and $u_h^{n+1} = R_\omega U_h^{n+1}$ with R_ω the restriction operator introduced in Section 2.1.

Starting from Problems (2.3) and (2.11), we get: $\forall V_h \in V_h^\Omega$,

$$a_\Omega(U_h^{n+1} - U^{n+1}, V_h) = \nu\delta t \; b(\lambda_{h'}^{n+1} - \lambda^{n+1}, V_h) + < U_h^n - U^n, V_h >_{L_2(\Omega)} . \tag{2.17}$$

From (2.6), using the first trace continuity theorem, i.e. $\forall V \in H^1_{\mathcal{P}}(\Omega)$, $||\gamma_0(R_\omega V)||_{H^{1/2}(\gamma)} \leq C_\gamma ||V||_{H^1(\Omega)}$, and the Cauchy-Schwartz inequality, it comes $\forall V_h \in V_h^\Omega$, $V_h \neq 0$,

$$\frac{a_\Omega(U_h^{n+1} - U^{n+1}, V_h)}{||V_h||_{H^1(\Omega)}} \leq \nu\delta t C_\gamma ||\lambda^{n+1} - \lambda_{h'}^{n+1}||_{H^{-1/2}(\gamma)} + ||U_h^n - U^n||_{L_2(\Omega)}. \tag{2.18}$$

From the ellipticity inequality (2.8), expression (2.18) leads to:

$$\xi ||U_h^{n+1} - U^{n+1}||_{H^1(\Omega)} \leq \nu\delta t C_\gamma ||\lambda^{n+1} - \lambda_{h'}^{n+1}||_{H^{-1/2}(\gamma)} + ||U_h^n - U^n||_{L_2(\Omega)}. \tag{2.19}$$

The continuity of the restriction operator R_ω from $H^1_{\mathcal{P}}(\Omega)$ to $H^1(\omega)$ gives

$$\frac{\xi}{K} ||u_h^{n+1} - u^{n+1}||_{H^1(\omega)} \leq \nu\delta t C_\gamma ||\lambda^{n+1} - \lambda_{h'}^{n+1}||_{H^{-1/2}(\gamma)} + ||U_h^n - U^n||_{L_2(\Omega)} \tag{2.20}$$

Since $\forall v \in H^1(\omega)$, $\int_\omega \nu\delta t \nabla(u_h^{n+1} - u^{n+1}) \nabla v dx dy + \int_\omega (u_h^{n+1} - u^{n+1}) v dx dy \leq max(1, \nu\delta t) \; ||u_h^{n+1} - u^{n+1}||_{H^1(\omega)} ||v||_{H^1(\omega)}$, (2.20) leads to,

$$\forall v \in H^1(\omega), \; v \neq 0, \; \frac{\xi}{max(1, \nu\delta t) \; K} \frac{\int_\omega \nabla(u_h^{n+1} - u^{n+1}) \nabla v dx dy}{||v||_{H^1(\omega)}} \leq \nu\delta t C_\gamma ||\lambda^{n+1} - \lambda_{h'}^{n+1}||_{H^{-1/2}(\gamma)} + ||U_h^n - U^n||_{L_2(\Omega)}. \tag{2.21}$$

Assuming enough regularity for $u_h^{n+1} - u^{n+1}$, i.e $u_h^{n+1} - u^{n+1} \in H^2(\omega)$ (we delay to Remark 2.1 some comments about the regularity of this quantity), we integrate by parts and (2.21) becomes, $\forall v \in H^1(\omega)$, $v \neq 0$,

$$\frac{\xi}{max(1, \nu\delta t) \; K} \frac{\int_\omega (I - \nu\delta t \Delta) \; (u_h^{n+1} - u^{n+1}) v dx dy + \nu\delta t \int_\gamma (\frac{\partial u_h^{n+1}}{\partial n_\gamma^+} - \frac{\partial u^{n+1}}{\partial n_\gamma^+}) \gamma_0(v) d\sigma}{||v||_{H^1(\omega)}} \leq \nu\delta t C_\gamma \quad ||\lambda^{n+1} - \lambda_{h'}^{n+1}||_{H^{-1/2}(\gamma)} + ||U_h^n - U^n||_{L_2(\Omega)}, \tag{2.22}$$

that leads to:

$$sup_{v\in H^1(\omega),v\neq 0}\frac{\int_\gamma(\frac{\partial u_h^{n+1}}{\partial n_\gamma^+}-\frac{\partial u^{n+1}}{\partial n_\gamma^+})\gamma_0(v)d\sigma}{||v||_{H^1(\omega)}} \leq \frac{1}{\nu\delta t}sup_{v\in H^1(\omega),v\neq 0}\frac{|\int_\omega(I-\nu\delta t\Delta)\ (u_h^{n+1}-u^{n+1})v|dxdy}{||v||_{H^1(\omega)}} + \frac{max(1,\nu\delta t)\ K}{\xi}C_\gamma||\lambda^{n+1}-\lambda_{h'}^{n+1}||_{H^{-1/2}(\gamma)} + \frac{max(1,\nu\delta t)\ K}{\xi}\frac{1}{\nu\delta t}||U_h^n-U^n||_{L_2(\Omega)}. \tag{2.23}$$

In order to conclude, it remains to show the two following inequalities:

$$1)\ sup_{v\in H^1(\omega),v\neq 0}\frac{\int_\gamma(\frac{\partial u_h^{n+1}}{\partial n_\gamma^+}-\frac{\partial u^{n+1}}{\partial n_\gamma^+})\gamma_0(v)d\sigma}{||v||_{H^1(\omega)}} \geq \beta'||\frac{\partial u_h^{n+1}}{\partial n_\gamma^+}-\frac{\partial u^{n+1}}{\partial n_\gamma^+}||_{H^{-1/2}(\gamma)},$$

$$2)\ sup_{v\in H^1(\omega),v\neq 0}\frac{|\int_\omega(I-\nu\delta t\Delta)\ (u_h^{n+1}-u^{n+1})vdxdy|}{||v||_{H^1(\omega)}} \leq c_1\nu\delta t||\lambda^n-\lambda_{h'}^n||_{H^{-1/2}(\gamma)} + c_2||U_h^{n-1}-U^{n-1}||_{L_2(\Omega)}.$$

First inequality:

Using the bounded linear restriction operator R_ω introduced in Section 2.1, it is straightforward that,

$$\forall\mu\in H^{-1/2}(\gamma),\ \forall V\in H^1(\Omega),\ V\neq 0,\ \frac{b(V,\mu)}{||V||_{H^1(\Omega)}}\leq K\frac{b(V,\mu)}{||R_\omega V||_{H^1(\omega)}}, \tag{2.24}$$

which provides, taking $\mu=\frac{\partial u_h^{n+1}}{\partial n_\gamma^+}-\frac{\partial u^{n+1}}{\partial n_\gamma^+}$ and assuming enough regularity (see Remark 2.1), $\forall V\in H^1(\Omega)$, $b(V,\frac{\partial u_h^{n+1}}{\partial n_\gamma^+}-\frac{\partial u^{n+1}}{\partial n_\gamma^+})=\int_\gamma(\frac{\partial u_h^{n+1}}{\partial n_\gamma^+}-\frac{\partial u^{n+1}}{\partial n_\gamma^+})\gamma_0(R_\omega V)d\sigma$,

$$sup_{V\in H^1(\Omega),V\neq 0}\frac{\int_\gamma(\frac{\partial u_h^{n+1}}{\partial n_\gamma^+}-\frac{\partial u^{n+1}}{\partial n_\gamma^+})\gamma_0(R_\omega V)d\sigma}{||V||_{H^1(\Omega)}}\leq K\ sup_{v\in H^1(\omega),v\neq 0}\frac{\int_\gamma(\frac{\partial u_h^{n+1}}{\partial n_\gamma^+}-\frac{\partial u^{n+1}}{\partial n_\gamma^+})\gamma_0(v)d\sigma}{||v||_{H^1(\omega)}}.$$

Combining this equation with the Inf-Sup condition (2.10), it comes:

$$sup_{v\in H^1(\omega),v\neq 0}\frac{\int_\gamma(\frac{\partial u_h^{n+1}}{\partial n_\gamma^+}-\frac{\partial u^{n+1}}{\partial n_\gamma^+})\gamma_0(v)d\sigma}{||v||_{H^1(\omega)}}\geq\frac{\beta}{K}||\frac{\partial u_h^{n+1}}{\partial n_\gamma^+}-\frac{\partial u^{n+1}}{\partial n_\gamma^+}||_{H^{-1/2}(\gamma)}, \tag{2.25}$$

which is the first inequality with $\beta'=\frac{\beta}{K}$.

Second inequality:

Introducing $(I-\nu\delta t\Delta)^{1/2}$ we get:

$$\int_\omega (I-\nu\delta t\Delta)(u_h^{n+1}-u^{n+1})vdxdy = \int (I-\nu\delta t\Delta)^{1/2}(u_h^{n+1}-u^{n+1})(I-\nu\delta t\Delta)^{1/2}vdxdy,$$

and, using the Cauchy Schwartz inequality:

$$|\int_\omega (I-\nu\delta t\Delta)(u_h^{n+1}-u^{n+1})vdxdy| \leq ||(I-\nu\delta t\Delta)^{1/2}(u_h^{n+1}-u^{n+1})||_{L^2(\omega)}||(I-\nu\delta t\Delta)^{1/2}v||_{L^2(\omega)}.$$

Since, due to norm equivalence, $||(I-\nu\delta t\Delta)^{1/2}w||_{L^2(\omega)} \leq C_E||w||_{H^1(\omega)}$, using the definitions of u_h^{n+1} and u^{n+1} we get the expected inequality.

Coming back to (2.23), we get,

$$||\frac{\partial u_h^{n+1}}{\partial n_\gamma^+} - \frac{\partial u^{n+1}}{\partial n_\gamma^+}||_{H^{-1/2}(\gamma)} \leq c||\lambda^n - \lambda_{h'}^n||_{H^{-1/2}(\gamma)} + \frac{c'}{\nu\delta t}||U_h^{n-1}-U^{n-1}||_{L_2(\Omega)}, \tag{2.26}$$

with $c = \frac{2max(1,\nu\delta t)K(1+C_E)c_\gamma}{\beta\xi}$ and $c' = \frac{2max(1,\nu\delta t)K(1+C_E)}{\beta\xi}$. Note that as soon as $\nu\delta t < 1$ (which is usually the case), neither the constant c nor the constant c' depend on δt.

Similarly, one can prove that,

$$||\frac{\partial R_{\Omega\setminus\bar{\omega}}U^{n+1}}{\partial n_\gamma^-} - \frac{\partial R_{\Omega\setminus\bar{\omega}}U_h^{n+1}}{\partial n_\gamma^-}||_{H^{-1/2}(\gamma)}) \leq c||\lambda^n - \lambda_{h'}^n||_{H^{-1/2}(\gamma)} + \frac{c'}{\nu\delta t}||U_h^{n-1}-U^{n-1}||_{L_2(\Omega)}, \tag{2.27}$$

that concludes the proof.

■

Remark 2.1. Regularity estimates on any open sub-domain included in ω can be obtained straightforward remarking that the restriction of u on any sub-domain is solution of a Dirichlet problem.

Remark 2.2.

Theorem 2.1 relates the error on the normal gradient jump at the boundary of the domain to the approximation errors for the Lagrange multipliers and the solution on the whole fictitious domain. According to [2], both approximation errors are controlled by the initial projection error in V_j and error terms of type 2^{-js} and

$2^{-j's'}$ related to the approximation scales and regularities for the solution and the Lagrange multipliers.

Numerically, we have focussed our attention on the influence of the quality of approximation of the space $Q_{j'}^{\gamma}$ on the quality of the normal gradient jump approximation. Figure 6 reports the L^2 error on the Lagrange multipliers versus the size $2^{j'}$ of the space $Q_{j'}^{\gamma}$. The expected evolution is the power law $2^{-m'j'}$ with $m' = 4$ plotted in dash line on the figure.

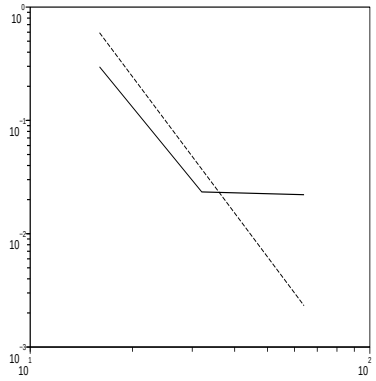

Fig. 6. L^2 error on the Lagrange multipliers versus the size $2^{j'}$ of the space $Q_{j'}^{\gamma}$ (log-log scale). The dash line stands for the expected theoretical decay (slope $-m' = -4$)

2.5. *Conclusion on the approach*

The different parts of this section have put into evidence many advantages of the proposed approach. Focussing on the quality of the approximation, it has been shown that optimal precision is reached in interior domains and that the low precision in the vicinity of the boundary can be tackled using adaptivity of the approximation spaces. Moreover, the use of wavelet type spaces for the approximation of the Lagrange multipliers induce a high precision level for the evaluation of normal gradient jumps.

It is known that Stefan problems are good challenges for numerical methods of the type presented above. In the sequel of this paper we present a new method, derived from the previous part for the simulation of Stefan like problems.

3. The continuous problem

From now, we consider the bi-dimensional Stefan problem in its simplest formulation, that can be associated to a change of phase (for instance the melting of a piece of ice). More specifically, we consider at time $t = t_0$, a bi-dimensional domain ω filled in by a liquid phase with a boundary γ, called the interface and surrounded by a solid phase ω_{so}. We note $\Omega = \bar{\omega} \cup \omega_{so}$ (see Figure 1).

It is assumed that a phase changing occurs in the vicinity of the boundary and therefore the interface γ and consequently ω are functions of time $t \in [t_0, T]$.

If we assume that the heat transfer is performed using the Fourier's law with a constant diffusivity and that the temperature of the solid phase is known (for instance the critical temperature), we get, after normalization, the following so called one phase problem:

$$\begin{cases} \text{Find } u \in C^1\left([t_0,T], C^2(\omega(t) \bigcap C^0(\bar{\omega}))\right) \text{ such that} \\ \frac{\partial u}{\partial t} - \nu \Delta u = f \text{ for } (x,y) \in \omega(t), t \in [t_0, T], \\ u|_{\gamma(t)} = g, \\ u(t_0, .) = u_0 \text{ on } \omega(t_0), \\ \frac{d\gamma}{dt} = -k \ \frac{\partial u}{\partial \mathbf{n}} \ \mathbf{n}, \\ \gamma(t = t_0) = \gamma_0, \end{cases} \tag{3.1}$$

where u is the temperature inside the domain ω and the vector $\mathbf{n}$ is the outward normal of γ. The initial position of the interface is γ_0 and u_0 stands for the initial temperature distribution. The function f stands for the heat source term and g is the temperature along the boundary γ. $\frac{\partial u}{\partial \mathbf{n}}$ denotes the normal derivative of u inside the liquid region and k is related to the thermal diffusivity of the liquid phase.

Classically, in weak formulations of the Stefan problem, the interface $\gamma(t)$ is represented in the form

$$\gamma(t) = \{(x,y) \in \Omega, \text{ such that } \mathcal{D}(t,x,y) = 0\}, \tag{3.2}$$

with $\mathcal{D}$ the so-called level set function ([25]) satisfying the following problem:

$$\begin{cases} \text{Find } \mathcal{D} \in C^1\left([t_0,T], C^1(\Omega)\right) \text{ such that} \\ \frac{\partial \mathcal{D}}{\partial t} + \mathbf{V}.\nabla \mathcal{D} = 0, \\ \mathcal{D}(t_0, .) = d_0, \end{cases} \tag{3.3}$$

where d_0 is the signed Euclidean distance to the interface γ_0 (d_0 is positive if the point is outside $\omega(t_0)$ and negative otherwise) and $\mathbf{V}$ stands for a continuous extension of $-k \ \frac{\partial u}{\partial \mathbf{n}} \ \mathbf{n}$ from γ onto Ω.

The continuous Stefan problem we are considering in this paper is formed by the system of equations (3.1) and (3.3) closed by (3.2).

Results on the existence and uniqueness of a classical solution of the Stefan problem with, in particular a control of the regularity of the interface γ can be found for instance in [19].

4. Discretization of the problem and approximation to the solution

The numerical algorithm we are presenting consists of a wavelet/fictitious domain solver for the approximation to the heat equation (3.1) coupled with a finite difference approximation to the interface evolution written in its (level set) weak form (3.3). At each time step t_n, a splitting of the problem leads to a convection problem for the interface with a fixed velocity $-k\ \frac{\partial u(t_n)}{\partial \mathbf{n}}\ \mathbf{n}$ and a parabolic problem inside a fixed domain $\omega(t_{n+1})$ (see Subsection 4.2). In such a formulation, it is quite clear that the quality of the approximation of the normal gradient of u is crucial.

The discretization of the parabolic part is similar to what has been presented in the previous sections. We focus here on the approximation of the interface evolution equation.

4.1. *Finite difference approximation to the interface evolution equation*

We focus in this section on the approximation of problem (3.3). We assume that $\mathbf{V}$ is known for any t and any position in Ω and we denote its components by $V_x(t,.)$ and $V_y(t,.)$.

The numerical realization of (3.3) uses a TVD scheme with flux limiters ([18]). This kind of scheme has been introduced to ensure a second order approximation scheme in space for the regular part of the solution while avoiding oscillations near the discontinuities of the solution. This last property is essential since, in the complete formulation of the Stefan problem, the position of the interface γ is defined as the zero level set of the function $\mathcal{D}$. Spurious numerical oscillations as well as uncontrolled smoothing of the function $\mathcal{D}$ would lead to less accurate approximation to γ.

The time evolution of $\mathcal{D}$ during a time step δt_B is obtained by the following scheme:

$$\left\{\begin{array}{l}\text{Find } \mathcal{D}^{n_B} = \{\mathcal{D}^{n_B}_{k_1,k_2}\}_{k_1,k_2} \text{ such that,}\\ \mathcal{D}^{n_B+1}_{k_1,k_2} = \mathcal{D}^{n_B}_{k_1,k_2} - \frac{\delta t_B}{\delta x}(A_x^+ \mathcal{D}^{n_B}_{k_1-1/2,k_2} + A_x^- \mathcal{D}^{n_B}_{k_1+1/2,k_2})\\ \qquad\qquad -\frac{\delta t_B}{\delta x}(F^{n_B}_{k_1+1/2,k_2} - F^{n_B}_{k_1-1/2,k_2})\\ \qquad\qquad -\frac{\delta t_B}{\delta y}(A_y^+ \mathcal{D}^{n_B}_{k_1,k_2-1/2} + A_y^- \mathcal{D}^{n_B}_{k_1,k_2+1/2})\\ \qquad\qquad -\frac{\delta t_B}{\delta y}(F^{n_B}_{k_1,k_2+1/2} - F^{n_B}_{k_1,k_2-1/2}),\end{array}\right. \tag{4.1}$$

where the expressions of the quantities A_x^+, A_x^-, A_y^+, A_y^- and of the fluxes $F^{n_B}_{k_1-1/2,k_2}$, $F^{n_B}_{k_1+1/2,k_2}$, $F^{n_B}_{k_1,k_2-1/2}$ and $F^{n_B}_{k_1,k_2+1/2}$ are recalled in the appendix.

Remark 4.1.
- The stability of the scheme is ensured through a CFL condition relating δt_B and the spatial steps, $\delta x,\ \delta y$. It can be written for each $n_B \geq 0$, as

$$\delta t_B < \min\left(\frac{\delta x}{max_{k_1,k_2}(|V^{n_B}_{x,k_1-1/2,k_2}|)}, \frac{\delta y}{max_{k_1,k_2}(|V^{n_B}_{y,k_1,k_2-1/2}|)}\right). \qquad (4.2)$$

Therefore, for each iteration of the scheme (4.1), the time step δt_B is automatically adapted to ensure condition (4.2).
Solving the equation (3.3) does not provide directly the position of the new boundary. The numerical resolution of (3.3) provides the grid points of Ω belonging to the new domain. In Section 5.2, we propose a reconstruction technique in order to get the new boundary from the information given by the Level Set function $\mathcal{D}$.

4.2. *Approximation to the Stefan problem*

The numerical realization of the systems (3.1) and (3.3) is then performed solving alternatively systems (2.12) and (4.1). More precisely, assuming that at time t_n the quantities $u(t_n,.)$ and γ_n are known, the estimate of γ_{n+1} is obtained following Subsection 4.1 where $\mathbf{V}^n$ is constructed as a continuous extension of $-k\frac{\partial u(t_n,.)}{\partial \mathbf{n}}\ \mathbf{n}$. Then, taking $\gamma = \gamma_{n+1}$, the heat equation is solved on the new domain ω_{n+1}, following Subsection 2.1.

5. Numerical implementation

In this section, we first describe the implementations of problems (2.12) and (4.1), then address the numerical coupling.

5.1. *Implementation of (2.12)*

To simplify the description of the implementation, problem (2.12) is first rewritten in an equivalent algebraic formulation.

5.1.1. *Linear system*

Identifying $\mathbf{U^j_h}$ (resp. $\Lambda^n_{j'}$) with the vector of coordinates of U^n_j (resp. of $\lambda^n_{j'}$) on an orthonormal basis of U^Ω_j (resp. on an orthonormal basis of $Q^\gamma_{j'}$), equation (2.12) is equivalent to the following linear system, written for the sake of simplicity in the non adaptive configuration, i.e. using the basis $\{\phi^\Omega_\alpha\}_{\alpha\in K_j}$ (resp. the basis $\{\phi^\gamma_{\alpha'}\}_{\alpha'\in K'_{j'}}$):

Given $\mathbf{U^0_j} = \left(\langle U^0, \phi^\Omega_\alpha\rangle_{L^2(\Omega)}\right)_{\alpha\in K_j}$,

$$\begin{cases} \text{Find } \mathbf{U^{n+1}_j} \in I\!R^{4^j} \text{ and } \Lambda^{n+1}_{j'} \in I\!R^{2^{j'}} \text{ such that} \\ \mathbf{U^{n+1}_j} + C^{n+1}\Lambda^{n+1}_{j'} = \mathbf{R^n_j}, \\ D^{n+1}\mathbf{U^{n+1}_j} = \mathbf{G^{n+1}_{j'}}, \end{cases} \qquad (5.1)$$

where

$$\left(\mathbf{R_j^n}\right)_\alpha = \langle U_j^n, \xi_\alpha^\Omega \rangle_{L^2(\Omega)} + < \delta t F^n, \xi_\alpha^\Omega >_{L^2(\Omega)} \tag{5.2}$$

$$\left(\mathbf{G_{j'}^{n+1}}\right)_{\alpha'} = \langle g^{n+1}, \phi_{\alpha'}^{\gamma_n} \rangle_{L^2(\gamma_{n+1})} \tag{5.3}$$

$$C_{\alpha,\alpha'}^{n+1} = -\nu\delta t \langle tr^{n+1}\left(R_{\omega_{n+1}}\xi_\alpha^\Omega\right), \phi_{\alpha'}^{\gamma_{n+1}} \rangle_{L^2(\gamma_{n+1})} \tag{5.4}$$

$$D_{\alpha',\alpha}^{n+1} = < tr^{n+1}(R_{\omega_{n+1}}\phi_\alpha^\Omega), \phi_{\alpha'}^{\gamma_{n+1}} >_{L^2(\gamma_{n+1})}, \tag{5.5}$$

with $tr^{n+1}(.)$ the first trace operator on γ_{n+1} and ξ_α^Ω, the function introduced in Section 2.1. Classically, the Uzawa algorithm (see e.g. [27]) is used to compute the solution of (5.1). This algorithm can be seen as a descent algorithm performed on the algebraic system of equations,

$$\left(D^{n+1}C^{n+1}\right)^t D^{n+1}C^{n+1}\Lambda_{j'}^{n+1} = \left(D^{n+1}C^{n+1}\right)^t D^{n+1}\mathbf{R_j^n} - \left(D^{n+1}C^{n+1}\right)^t \mathbf{G_{j'}^{n+1}} \tag{5.6}$$

and followed by computing $\mathbf{U_j^{n+1}} = \mathbf{R_j^n} - C^{n+1}\Lambda_{j'}^{n+1}$.

Remark 5.1.
The choice of a Petrov-Galerkin discretization leads to a linear system with the identity matrix as stiffness matrix, in contrast to what classically appears when using a Galerkin discretization ([17]). The difficulty associated to the resolution of a possibly ill-conditioned linear system is therefore circumvented. Note that the ill-conditioning of the differential operator appears in the change of bases at each iteration which is an operation for which a diagonal preconditioner classically exists in wavelet bases. However, due to the trace operator properties, the matrix $D^{n+1}C^{n+1}$ is ill-conditioned. A preconditioner for the iteration matrix $\left(D^{n+1}C^{n+1}\right)^t D^{n+1}C^{n+1}$ (diagonal within the wavelet framework) has been proposed in [2].

5.1.2. *Choice of the multi-resolutions*

We introduce the multi-resolution analysis used for the practical implementation.

- The multi-resolution analysis associated to Ω (i.e. $\{U_j^\Omega\}_{j\in\mathbb{Z}}$) is a (L, L')-periodic orthonormal m-order spline multi-resolution analysis ([26]) constructed by tensor product.

- The multi-resolution analysis associated to γ_n (i.e. $\{Q_{j'}^{\gamma_n}\}_{j'\in\mathbb{Z}}$) is the image on γ_n, using a piecewise C^1-transform, of the m'-order multi-resolution related to orthonormal compactly supported wavelet bases introduced in [13] and adapted to the interval in [12] and [8].
  More precisely, if $\mathcal{H}_n$: $\mathbb{R} \to \mathbb{R}^2$ denotes the piecewise C^1-transform such that,

$$\gamma_n = \mathcal{H}_n([0,1]), \tag{5.7}$$

we define $\phi_0^{\gamma_n}$ as,

$$\forall s \in \gamma_n,\ \phi_0^{\gamma_n}(s) = \phi_0^{[0,1]}(\mathcal{H}_n^{-1}(s)), \tag{5.8}$$

where $\phi_0^{[0,1]}$ is the scaling function of the multi-resolution on the interval.

Observe that the multi-resolution spanned by $\phi_0^{\gamma_n}$ inherits all the properties of a multi-resolution of $L^2(\gamma_n)$ except the orthonormality of the family $\{\phi_{\alpha'}^{\gamma_n}\}_{\alpha' \in K'_{j'}}$ in the classical L^2-sense. However, since the Jacobian $J_{\mathcal{H}_n}$ of the transform is assumed to be bounded, the orthonormality of this family is ensured in the $L^2_{\mathcal{H}_n}$-sense such that,

$$\forall (f,g) \in L^2(\gamma_n),\ \langle f,g\rangle_{L^2_{\mathcal{H}_n}(\gamma)} = \int_\gamma f(s)\bar{g}(s)|J_{\mathcal{H}_n^{-1}}(s)|ds. \tag{5.9}$$

In our numerical tests, $\mathcal{H}_n$ is the transform associated to the construction of a piecewise linear approximation to γ_n.

5.1.3. *Computation of the terms in (5.1)*

Solving numerically (5.1) involves two kinds of calculations, namely:
1) Pre-calculations consisting, on one hand, in the extension of the initial condition u_0 to the whole domain Ω and, on the other hand, in the computation of filters of the form $\{\langle \phi_{\alpha_1}^{\Omega}, \xi_{\alpha_2}^{\Omega}\rangle_{L^2(\Omega)},\ (\alpha_1,\alpha_2) \in K_j \times K_j\}$.
2) Evaluation at each time step of the matrices D^{n+1} and C^{n+1} and of the right-hand-side terms of (5.1) using (5.2)-(5.5).

1) **Pre-calculations:**

- The Uzawa algorithm is initialized by constructing U^0, an extension of the initial condition u_0 from ω to the whole domain Ω. This extension is an important point that controls the regularity of the solution around the boundary γ. However, the discussion about different extension procedures is out of the scope of this work; spectral embedding have been developed for instance in [14] and extensions using multi-resolutions on the interval are currently investigated. In the tests presented in this paper, low cost extensions will be used.

The computation of the following quantities,

$$(\mathbf{U_j^0})_\alpha = \langle U^0, \phi_\alpha^{\Omega}\rangle_{L^2(\Omega)},\ \alpha \in K_j \tag{5.10}$$

is then performed using an interpolation filter ([26]) that relates the scaling coefficients of the spline interpolation of U^0 to its point values.

- The computation of filters of the form $\{\langle\phi^{\Omega}_{\alpha_1},\xi^{\Omega}_{\alpha_2}\rangle_{L^2(\Omega)},\ (\alpha_1,\alpha_2)\in K_j\times K_j\}$ is performed once and for all using the explicit expression of the Fourier transforms of $\phi^{\Omega}_{\alpha_1}$ and $\xi^{\Omega}_{\alpha_2}$ following [9].

2) **Evaluation at each time step:**

- Assembling of the matrices D^{n+1} and C^{n+1}:

We recall that the coefficients of D^{n+1} and C^{n+1} are given by,

$\forall(\alpha,\alpha')\in K_j\times K'_{j'}$,

$$D^{n+1}_{\alpha',\alpha}=\int_{\gamma_{n+1}}\phi^{\Omega}_{\alpha}(s)\phi^{\gamma_{n+1}}_{\alpha'}(s)ds, \tag{5.11}$$

$$C^{n+1}_{\alpha,\alpha'}=\int_{\gamma_{n+1}}\xi^{\Omega}_{\alpha}(s)\phi^{\gamma_{n+1}}_{\alpha'}(s)ds, \tag{5.12}$$

where we write $tr^{n+1}(R_{\omega_{n+1}}\phi^{\Omega}_{\alpha})(s)=\phi^{\Omega}_{\alpha}(s)$ (resp. $tr^{n+1}(R_{\omega_{n+1}}\xi^{\Omega}_{\alpha})(s)=\xi^{\Omega}_{\alpha}(s)$). Using (5.8), expressions (5.11) and (5.12) become,

$$D^{n+1}_{\alpha',\alpha}=\int_{[0,1]}\phi^{\Omega}_{\alpha}(\mathcal{H}_{n+1}(\tau))\phi^{[0,1]}_{\alpha'}(\tau)\mid J_{\mathcal{H}_{n+1}}(\tau)\mid d\tau, \tag{5.13}$$

$$C^{n}_{\alpha,\alpha'}=\int_{[0,1]}\xi^{\Omega}_{\alpha}(\mathcal{H}_{n+1}(\tau))\phi^{[0,1]}_{\alpha'}(\tau)\mid J_{\mathcal{H}_{n+1}}(\tau)\mid d\tau. \tag{5.14}$$

The evaluation of these two quantities is efficiently performed exploiting tree algorithms related to multi-resolutions, classical results of spline theory (particularly, a fast iterative algorithm to evaluate point values of B-spline ([10])) as well as quadrature formula and tree algorithms related to wavelets on the interval ([11], [8]).

- Computation of the right-hand-side terms:

For any $n\geq 0$, knowing F^n, the quantities $\left(\mathbf{F^n_j}\right)_{\alpha}=\langle F^n,\phi^{\Omega}_{\alpha}\rangle_{L^2(\Omega)},\ \alpha\in K_j$ are first evaluated using an interpolation filter ([26]), then, knowing $\{\left(\mathbf{U^n_j}\right)_{\alpha}\}_{\alpha\in K_j}$, evaluated in the previous iteration, the right hand side $(\mathbf{R^n_j})_{\alpha},\ \alpha\in K_j$ (expression (5.2)) is evaluated as follows,

$$(\mathbf{R^n_j})_{\alpha}=\sum_{\alpha_1\in K_j}\left(\left(\mathbf{U^n_j}\right)_{\alpha_1}+\delta t\left(\mathbf{F^n_j}\right)_{\alpha_1}\right)\langle\phi^{\Omega}_{\alpha_1},\xi^{\Omega}_{\alpha}\rangle_{L^2(\Omega)}. \tag{5.15}$$

Finally, knowing $\forall n\geq 0$, $g(t_{n+1},.)$, the computation of the vector $\{\left(\mathbf{G^{n+1}_{j'}}\right)_{\alpha'}\}_{\alpha'\in K'_{j'}}$ (expression (5.3)) is performed using quadrature formula and tree algorithms.

5.2. *Implementation of (4.1)*

The technical difficulties related to the iteration of (4.1) are related to

- the initialization of the distance function at $t = t_0$ and the re-initialization of $\mathcal{D}^n$ after each time step (this procedure enforces $\mathcal{D}^n$ to be an exact distance function).
- the explicit construction of the interface.

We describe the solutions that we proposed to these difficulties in the sequel of this subsection.

For the simplicity of our notations, we remove in the sequel the exponents related to the time dependency.

- Evaluation of $\mathcal{D}^n$:

The level set function $\mathcal{D}$ is initialized at time $t = t_0$ and reinitialized at each time $t = t_n$, $n = 1, 2, \ldots$, by the following signed distance function:

$$\mathcal{D}^* = \begin{cases} d \text{ in } \omega, \\ -d \text{ in } \Omega \setminus \omega, \\ 0 \text{ on } \gamma, \end{cases} \tag{5.16}$$

where d is the Euclidean distance to γ. At each time step, knowing $\mathcal{D}$, the function $\mathcal{D}^*$ is obtained iterating the equation

$$\frac{\partial \mathcal{D}^*}{\partial t} = S_{\varepsilon_0}(\mathcal{D})(1 - |\nabla \mathcal{D}^*|)$$

to steady state, where $S_{\varepsilon_0}(\mathcal{D}) = \sqrt{\mathcal{D}^2 + \varepsilon_0^2}$ is the smoothed sign function of $\mathcal{D}$. At $t = t_0$, $\mathcal{D}$ is any arbitrary function positive in ω, negative outside of $\overline{\omega}$ and zero on γ. At any $t > t_0$, $\mathcal{D}$ is the output of the numerical approximation of (5.1). More details can be seen in [7]. Another possible solution for initialization and re-initialization is described in Remark 5.2.

- Explicit construction of the interface:

Replacing $\mathcal{D}$ by the piecewise bilinear interpolation of $\mathcal{D}$ over the grid, the corresponding interface γ, defined as the zero level set of $\mathcal{D}$ is then determined using the following steps, assuming that it is a smooth and closed curve:

(*i*) Computation of P_γ the family of points which lie on the grid lines and satisfy the condition $\mathcal{D} = 0$.

(*ii*) Ordering of P_γ to minimize the length of the corresponding boundary γ, i.e., to minimize $\sum_{i=1}^{n_\gamma} dist(P_\gamma^i, P_\gamma^{i+1})$ with $P_\gamma^{n_\gamma+1} = P_\gamma^1$ and n_γ the cardinal of P_γ.

(*iii*) Construction of the piecewise linear boundary γ connecting points from the ordered family P_γ.

5.3. *Coupling*

The key points of the numerical coupling between (5.1) and (4.1) is the extension of the convection velocity $\mathbf{V} = (V_x, V_y)^t = -k\frac{\partial u}{\partial \mathbf{n}}\ \mathbf{n}$ in a sufficiently large domain around the interface. Since the normal gradient of u is only relevant in ω and along the interface γ, specific extensions of V_x and V_y are required. Again for simplicity of our notations, we remove the time dependency.

The normal velocity $\frac{\partial u}{\partial \mathbf{n}}$ on γ is computed using the second order one-sided finite differences at the points P_γ and extended linearly onto the whole boundary γ. Then the approximations of V_x and V_y is extended into a neighborhood of γ as follows:

The points of P_γ are first translated along the local normal at a distance δ in both outer and inner directions. This provides two families of points P_γ^+ and P_γ^- and, by linear interpolation two boundaries called γ^- and γ^+. It also provides an extension of V_x and V_y on these boundaries. Finally, if Ξ_γ stands for the domain bounded by the boundaries γ^- and γ^+, an extension of V_x and V_y on Ξ_γ is performed after triangulation of Ξ_γ with triangles using edges of γ^-, γ and γ^+ and piecewise linear interpolation.

Remark 5.2. The above described procedure can also be used to initialize/reinitialize the distance function $\mathcal{D}^*$.

Indeed, if $\mathcal{D}_\tau = \begin{cases} \delta \text{ on } \gamma^+, \\ 0 \text{ on } \gamma, \\ -\delta \text{ on } \gamma^- \end{cases}$ is the piecewise linear approximation of the exact signed distance function constructed over the triangulation τ, the function $\mathcal{D}^*$ can be defined as follows:

$\mathcal{D}^* = \begin{cases} \mathcal{D}_\tau \text{ in } \Xi_\gamma, \\ \delta \text{ in } \omega \setminus \Xi_\gamma, \\ -\delta \text{ in } \Omega \setminus (\Xi_\gamma \cup \omega). \end{cases}$ Here, γ is computed using $\mathcal{D}$.

5.4. *Description of the algorithm*

The global sketch of the resolution algorithm can be written as follows,

Algorithm for solving the Stefan problem

- Choice of the parameters: $m,\ m',\ j,\ j', \delta t$.

Pre-calculations

- Evaluation of the filters $\{\langle \phi^{\Omega}_{\alpha_1}, \xi^{\Omega}_{\alpha_2} \rangle_{L^2(\Omega)}\},\ (\alpha_1, \alpha_2) \in K_j \times K_j$.
- Extension of u_0 on Ω and evaluation of $\mathbf{U_j^0}$.

Iteration, $n \geq 0$

- Evaluation of $\mathbf{V}^n$ and extension into Ω.
- Construction of the new boundary,

$$(\gamma_n, \mathbf{V}^n, \delta t, j, n) \ \rightarrow \ \gamma_{n+1}.$$

- Computation of $D^{n+1}, C^{n+1}, \mathbf{R_j^n}, \mathbf{G_{j'}^{n+1}}$.
- Solving by a gradient-type minimization method,

$$\left(D^{n+1}C^{n+1}\right)^t D^{n+1}C^{n+1}\Lambda_{j'}^{n+1} = \left(\mathrm{D^{n+1}C^{n+1}}\right)^{\mathrm{t}} \mathrm{D^{n+1}}\mathbf{R_j^n} - \left(\mathrm{D^{n+1}C^{n+1}}\right)^{\mathrm{t}} \mathbf{G_{j'}^{n+1}},$$

and then computing $\mathbf{U_j^{n+1}} = \mathbf{R_j^n} - \mathrm{C^{n+1}}\Lambda_{\mathrm{j'}}^{\mathrm{n+1}}$.

5.5. *Complexity analysis*

For the sake of simplicity, the complexity of the algorithm is evaluated for the full (non adapted) space of approximation U_j^{Ω}, i.e for a regular grid of step size 2^{-j} covering the fictitious domain Ω. Each step of the previous algorithm is considered:

- Pre calculations: Thanks to the translation invariance, the evaluation of the filters $\{< \phi^{\Omega}_{\alpha_1}, \xi^{\Omega}_{\alpha_2} >_{L^2(\Omega)}\},\ (\alpha_1, \alpha_2) \in K_j \times K_j$ can be performed, following [9] in $O(j)$ operations. Since there is no specific technique used for the extension into Ω, the global cost associated to this step remains $O(j)$.
- Iteration:
  Evaluation of $\mathbf{V}^n$ and extension into Ω: Since the evaluation is performed using an explicit finite difference method in a ring containing the boundary γ, it involves $O(2^j)$ operations.
  Construction of the new boundary: It is performed solving an explicit finite difference system on the regular grid covering Ω. Therefore, the associated

complexity is $O(4^j)$.
Computation of $D^{n+1}, C^{n+1}, \mathbf{R_j^n}, \mathbf{G_{j'}^{n+1}}$: Following [2], the computation of the matrices D^{n+1}, C^{n+1} involves $O(j2^{j+j'})$ operations, thanks to the localization of the B splines. The evaluation of $\mathbf{R_j^n}$ is performed in $O(2^j)$ operations while the evaluation of $\mathbf{G_{j'}^{n+1}}$ involves $O(2^{j'})$ operations, the constants being function of the length of the boundary γ.
Solution of the system: The saddle point problem is numerically solved in $O(2^{j'} + 4^j)$ operations, the constant being dependent on the number of iterations to reach convergence. Thanks to preconditioning, this number of iterations remains uniformly bounded.

Finally, taking into account that, thanks to the LBB condition $j' \leq j$, the global complexity of this algorithm is $O(j2^{j+j'} + 4^j)$. Note that for a fully adaptive version of this algorithm, 4^j should be replaced, in the previous estimate, by the dimension of the adapted approximation space (see the numerical examples of Section 6).

6. Numerical examples

In this section, we illustrate the efficiency of the presented approach for solving the Stefan problem defined in (3.1)-(3.3) on three model examples with known exact solutions. In all examples, the fictitious domain Ω is the unit square.

6.1. *Linear interface*

This problem is essentially univariate and corresponds, in the plane, to a linear interface that moves with a constant velocity.

Here, $\omega =]x_0, X_0[\times]0,1[$, $\nu = 1$, $k = 1$ and $f = 0$. The initial condition for the heat equation is $\forall (x,y) \in \omega_0 =]t_0, X_0[\times]0,1[$, $u_0(x,y) = e^{t_0 - x} - 1$. The boundary conditions are $u = 0$ on the line $x = x_0$ and $u = e^{t - X_0} - 1$ on the line $x = X_0$ (see Figure 7). Periodic boundary conditions are applied on the lower and upper parts of the boundary.

The exact solution to this Stefan problem is given by

$$\begin{cases} u(t,x,y) = e^{t-x} - 1, \\ \quad x_0(t) = t. \end{cases} \tag{6.1}$$

In Figure 8, we plot the computed values of $x_0(t)$ and cross-sections of the solution $u(t,x,y)$ at times $t = 0.315,\ 0.375,\ 0.45$. In this test, $t_0 = 0.3$, $X_0 = 0.75$. The computational parameters are $j = 6$, $j' = 4$, $m = m' = 4$, $\delta t = 0.015$. Note that the restriction of the solution to ω remains a nice approximation of $u(t,x,y) = e^{t-x} - 1$.

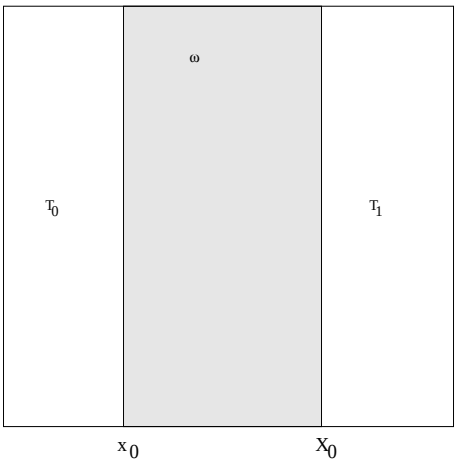

Fig. 7. Geometry for the Stefan problem (Section 6.1).

6.2. *Circular interface*

Here, we consider a ring shaped domain $\omega(t)$ (see Figure 9) where the interior boundary γ_f is a fixed circle of radius R_f while the exterior boundary γ_m is a moving circle of radius $R_m(t)$. Introducing polar coordinates $\theta,\ \rho$, the problem reads

$$\begin{cases} \frac{\partial u}{\partial t} - \Delta u = (2 - \frac{1}{\rho}) e^{R_{max} - \rho - t}, \\ u = 1 - e^{R_{max} - R_f - t} \ \text{ on } \gamma_f, \\ u = 0 \ \text{ on } \gamma_m, \\ u(t_0, \rho) = 1 - e^{R_{max} - \rho - t_0}, \\ \frac{dR_m}{dt} = -\frac{\partial u}{\partial \rho} \\ R_m(t_0) = R_{max}. \end{cases} \tag{6.2}$$

Its solution is given by

$$\begin{cases} u(t, \rho) = 1 - e^{R_{max} - \rho - t}, \\ R_m(t) = R_{max} - t. \end{cases} \tag{6.3}$$

The parameters of the simulation are $R_{max} = 0.4$, $R_f = 0.15$, $t_0 = 0.25$, $j = 6$, $j' = 4$, $m = m' = 4$, $\delta t = 0.001$. Figure 10 displays the evolution of the interface, as well as the wavelet coefficients of the solution on Ω. Clearly, dynamically adaptive approximation is required on the interface.

The evaluation of the L^2 error related to the approximation of the circular interface for different values of j is provided in Table 1. It shows that the estimate of the interface is numerically correct.

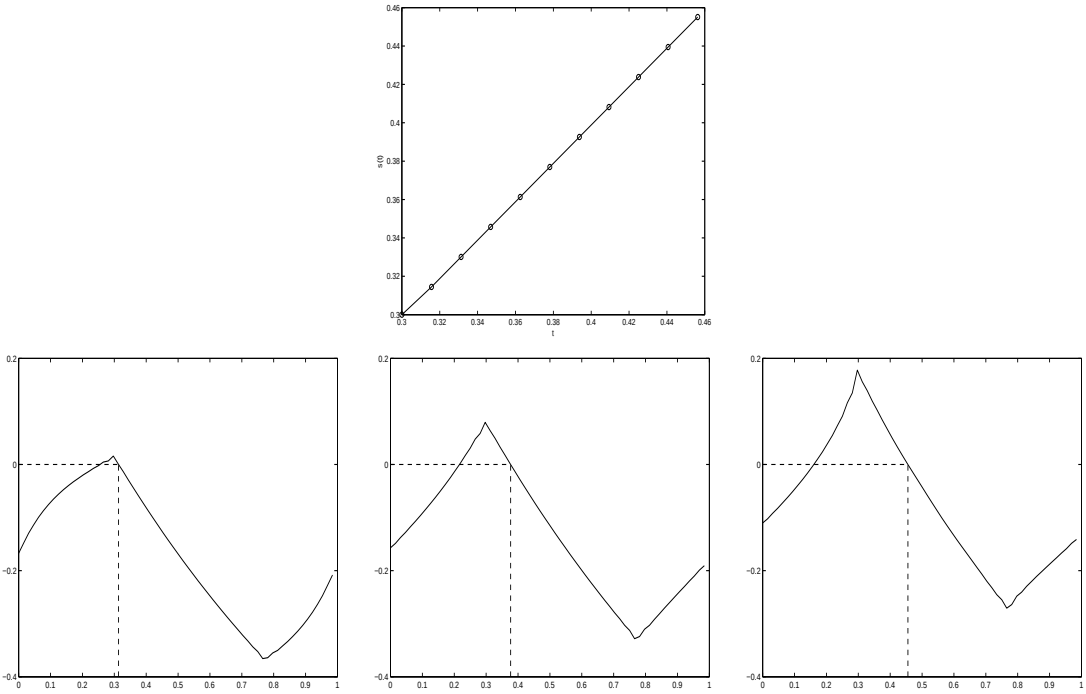

Fig. 8. Solution of the test problem of Section 6.1. Top: $x_0(t)$ (circle: computed, line: exact), Bottom: from left to right, cross-sections of the solution of the heat equation for $t = 0.315$,$t = 0.375$ and $t = 0.45$, the dashed line stands for the position of the moving boundary, recalling that, on the side $x = X_0$, the boundary is fixed.

L^2 error	Scale parameter j
1.34 10^{-2}	6
4.3 10^{-3}	7
3.9 10−3	8

Table 1. Least square error for the approximation of the circular interface versus j (Section 6.2)

6.3. *Sinusoidal interface*

Following [31] and [30], we consider in this example a problem similar to the previous one but with a sinusoidal perturbation of the external circular interface of the form:

$$R_m(t_0) = \overline{R}_m + \epsilon_p sin(K\theta), \tag{6.4}$$

where ϵ_p and K characterize the initial perturbation of the circular interface.

The linear stability analysis of [30] shows that the Stefan problem considered here leads to an amplification of the initial perturbation of the form $\epsilon_p e^{-\lambda t} sin(K\theta)$. Vari-

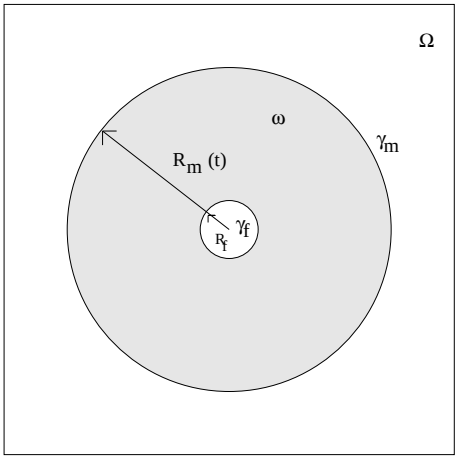

Fig. 9. Geometry for the Stefan problem (Section 6.2).

ous numerical estimates of the interface are reported on Figure 11-left for $\overline{R}_m = 0.4$, $\epsilon_p = 2.2e-2$ and $K = 10$, illustrating the fact that the initial perturbations of the interface rapidly increase. Figure 11-right shows that the quality of the approximation of the Lagrange multipliers is indeed a crucial point for such a problem (see section 2.4 and figure 6).

As mentioned in [2] and studied in [21], it is known that for the elliptic case Lagrange multiplier fictitious domain method, non-zero Lagrange multipliers imply a jump of the normal derivative in the vicinity of the boundary. Therefore, the solution belongs at most to the Sobolev space $H^{3/2-\varepsilon}, \varepsilon > 0$. Classically, this leads to the fact that the best N-term approximation in a wavelet basis [b] converges to the solution with an L^2 error of order $O(N^{-3/2+\varepsilon})$. Figure 12 exhibits for a fixed time $t_n = 0.1$, the L^2 error associated to the best N-term approximation of U_j^n with the periodic spline wavelets of order $m = 4$. Clearly the $N^{-3/2}$ scaling is noticeable and we can therefore guess that the regularity estimate is also valid in our case.

One can find on Figure 13 the position of the best 1063 wavelet coefficients associated to an L^2 error on $U_j^n, j = 6$ of 10^{-4}. Comparing to the approximatively 1600 coefficient associated to a regular grid of step size 2^{-6} covering ω or comparing to the 4096 coefficients associated to the regular approximation on Ω, one can conclude that the adaptive method is efficient.

[b] if $f = \sum_{\lambda \in \Lambda} c_\lambda \Psi_\lambda$ and if $\Phi : I\!N \to \Lambda$ is a sorting of the coefficient vector $\{|c_\lambda|\}$ in the decreasing order, the best N term approximation of f is $f_N = \sum_{i=1}^{N} c_{\Phi(i)} \Psi_{\Phi(i)}$.

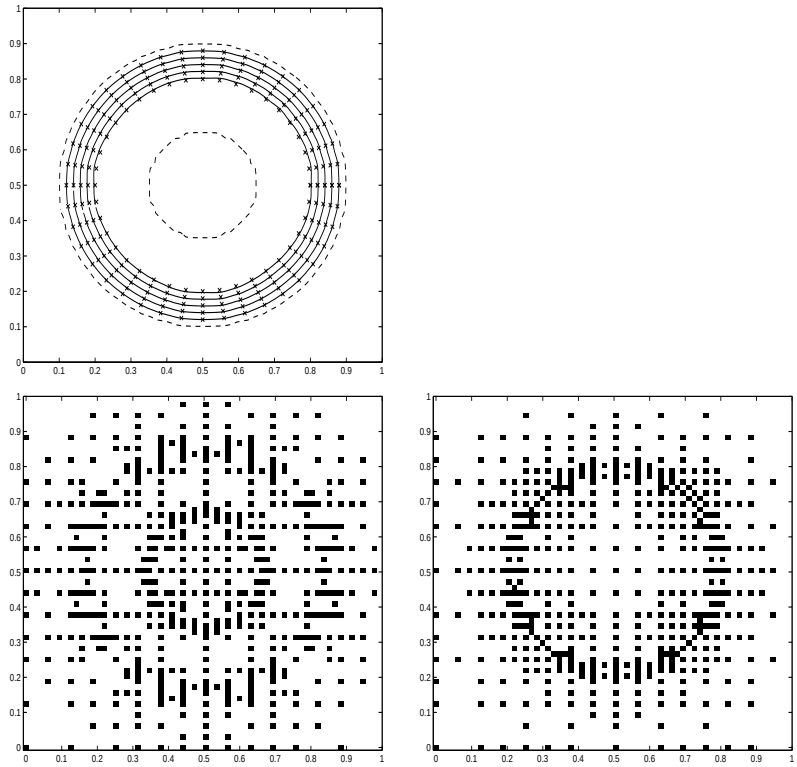

Fig. 10. Solution of the test problem of Section 6.2. Top: evolution of the interface, from $t = 0.02$ to $t = 0.1$, $--$: initial boundaries γ_m and γ_f, xx: exact interface, —: computed interface. Bottom: from left to right, wavelet decomposition of the solution at $t = 0$ and $t = 0.1$. Every wavelet coefficient $< U^n, \psi_\alpha^{\Omega,i} >_{L^2(\Omega)}$ with a modulus larger than $2\ 10^{-5}$ is depicted as a small black square.

7. Conclusion

After deriving various theoretical and numerical results on errors related to a recently developed numerical method for the approximation of stationary elliptic problems, a new numerical method for solving Stefan like problems has been presented. This method is based on the combination of a wavelets/fictitious domain method to solve the heat equation in a general domain with a level set method for evolving its boundary.

The described implementation together with achieved results point out the efficiency of this approach which follows among others from the combination of fast and accurate approximations and preconditioning properties together with suitable evaluation of the trace operators. This efficiency is amplified in situations where high adaptivity (grid refinement) is required.

Future developments will be devoted to analysis of simulations requiring high

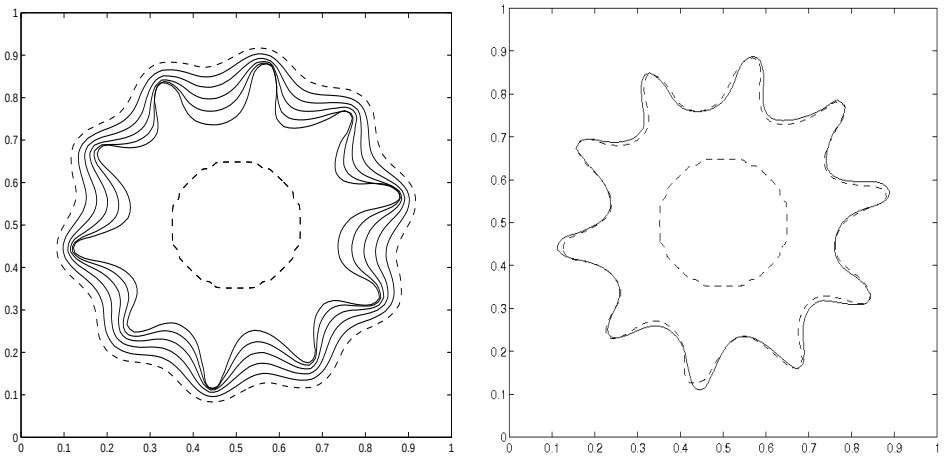

Fig. 11. Left: Instabilities generated by an initial perturbation of the interface. Initial boundaries γ_f and γ_m are depicted by dashed lines (Section 6.3). Right: Influence of the quality of approximation of $Q^{\gamma}_{j'}$;— $m' = 4$,−− $m' = 2$.

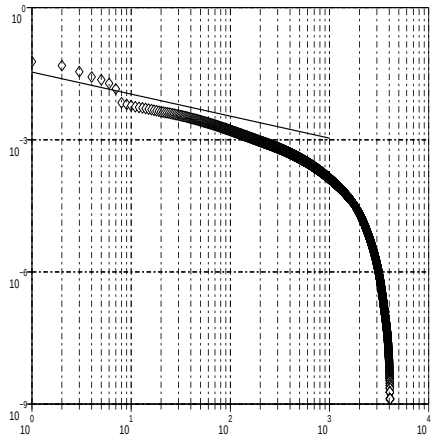

Fig. 12. Perturbed circular interface (Section 6.3), $t_n = 0.1, j = 6$. $\diamond$:L^2 error versus N for the best N-term approximation of U^n_j. Solid line: $N^{-3/2}$

precision and adaptivity, such as dendritic growth as well as to the development of a specific level set method incorporating highly adapted grids related to the wavelet approximation.

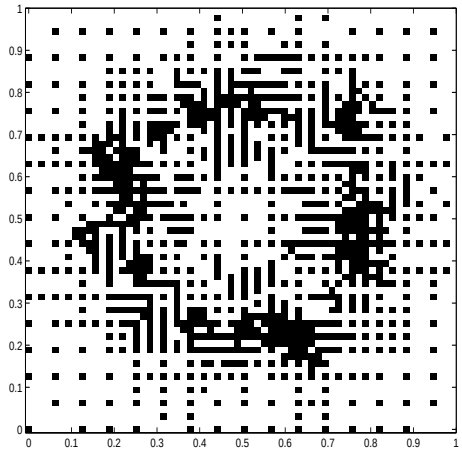

Fig. 13. Perturbed circular interface (Section 6.3). Position of the best $N = 1063$ wavelet coefficients corresponding to an error of 10^{-4}.

8. APPENDIX

The expressions of the quantities introduced in the numerical scheme for the evolution of the level set function $\mathcal{D}$ are reported. More details on the second order TVD scheme used in our code can be found in [18].

The quantities A_x^+, A_x^-, A_y^+, A_y^- are defined as follows:

$$A_x^+ \mathcal{D}^{n_B}_{k_1-1/2,k_2} = \begin{cases} V^{n_B}_{x,k_1-1/2,k_2} \left(\mathcal{D}^{n_B}_{k_1,k_2} - \mathcal{D}^{n_B}_{k_1-1,k_2} \right), \text{ if } V^{n_B}_{x,k_1-1/2,k_2} > 0, \\ 0, \text{ otherwise,} \end{cases} \tag{8.1}$$

$$A_x^- \mathcal{D}^{n_B}_{k_1+1/2,k_2} = \begin{cases} V^{n_B}_{x,k_1+1/2,k_2} \left(\mathcal{D}^{n_B}_{k_1+1,k_2} - \mathcal{D}^{n_B}_{k_1,k_2} \right), \text{ if } V^{n_B}_{x,k_1+1/2,k_2} < 0, \\ 0, \text{ otherwise,} \end{cases} \tag{8.2}$$

$$A_y^+ \mathcal{D}^{n_B}_{k_1,k_2-1/2} = \begin{cases} V^{n_B}_{y,k_1,k_2-1/2} \left(\mathcal{D}^{n_B}_{k_1,k_2} - \mathcal{D}^{n_B}_{k_1,k_2-1} \right), \text{ if } V^{n_B}_{y,k_1,k_2-1/2} > 0, \\ 0, \text{ otherwise,} \end{cases} \tag{8.3}$$

$$A_y^- \mathcal{D}^{n_B}_{k_1,k_2+1/2} = \begin{cases} V^{n_B}_{y,k_1,k_2+1/2} \left(\mathcal{D}^{n_B}_{k_1,k_2+1} - \mathcal{D}^{n_B}_{k_1,k_2} \right), \text{ if } V^{n_B}_{y,k_1,k_2+1/2} < 0, \\ 0, \text{ otherwise.} \end{cases} \tag{8.4}$$

Further, the fluxes $F^{n_B}_{k_1-1/2,k_2}$ and $F^{n_B}_{k_1,k_2-1/2}$ are computed as follows.

$$F^{n_B}_{k_1-1/2,k_2} = \frac{1}{2}|V^{n_B}_{x,k_1-1/2,k_2}|(1 - \frac{\delta t_B}{\delta x}|V^{n_B}_{x,k_1-1/2,k_2}|)W^{n_B}_{k_1-1/2,k_2}, \tag{8.5}$$

$$F^{n_B}_{k_1,k_2-1/2} = \frac{1}{2}|V^{n_B}_{y,k_1,k_2-1/2}|(1 - \frac{\delta t_B}{\delta y}|V^{n_B}_{y,k_1,k_2-1/2}|)W^{n_B}_{k_1,k_2-1/2}, \tag{8.6}$$

where

$$W^{n_B}_{k_1-1/2,k_2} = g(q^{n_B}_{k_1-1/2,k_2})(\mathcal{D}^{n_B}_{k_1,k_2} - \mathcal{D}^{n_B}_{k_1-1,k_2}), \tag{8.7}$$

$$W^{n_B}_{k_1,k_2-1/2} = g(q^{n_B}_{k_1,k_2-1/2})(\mathcal{D}^{n_B}_{k_1,k_2} - \mathcal{D}^{n_B}_{k_1,k_2-1}) \tag{8.8}$$

with

$$q^{n_B}_{k_1-1/2,k_2} = \begin{cases} \frac{\mathcal{D}^{n_B}_{k_1-1,k_2} - \mathcal{D}^{n_B}_{k_1-2,k_2}}{\mathcal{D}^{n_B}_{k_1,k_2} - \mathcal{D}^{n_B}_{k_1-1,k_2}}, \text{ if } V^{n_B}_{x,k_1-1/2,k_2} > 0, \\ \frac{\mathcal{D}^{n_B}_{k_1+1,k_2} - \mathcal{D}^{n_B}_{k_1,k_2}}{\mathcal{D}^{n_B}_{k_1,k_2} - \mathcal{D}^{n_B}_{k_1-1,k_2}}, \text{ if } V^{n_B}_{x,k_1-1/2,k_2} < 0, \end{cases} \tag{8.9}$$

$$q^{n_B}_{k_1,k_2-1/2} = \begin{cases} \frac{\mathcal{D}^{n_B}_{k_1,k_2-1} - \mathcal{D}^{n_B}_{k_1,k_2-2}}{\mathcal{D}^{n_B}_{k_1,k_2} - \mathcal{D}^{n_B}_{k_1,k_2-1}}, \text{ if } V^{n_B}_{y,k_1,k_2-1/2} > 0, \\ \frac{\mathcal{D}^{n_B}_{k_1,k_2+1} - \mathcal{D}^{n_B}_{k_1,k_2}}{\mathcal{D}^{n_B}_{k_1,k_2} - \mathcal{D}^{n_B}_{k_1,k_2-1}}, \text{ if } V^{n_B}_{y,k_1,k_2-1/2} < 0, \end{cases} \tag{8.10}$$

and g is a function defined by

$$g(q) = max(0, min(1, 2q), min(2, q)). \tag{8.11}$$

The remaining fluxes $F^{n_B}_{k_1+1/2,k_2}$ and $F^{n_B}_{k_1,k_2+1/2}$ are constructed by shifting indices.

References

1. D. Andreucci. Lecture notes on the stefan problem. *Doctorate course, Univ. La Sapienza*, 2002.
2. J. Baccou and J. Liandrat. Definition and analysis of a wavelet/fictitious domain solver for the 2d-heat equation on a general domain. *Math. Mod. and Meth. in Appl. Scien.*, 16(6):819–845, 2006.
3. J. Baccou and J. Liandrat. Interior estimates for wavelet petrov galerkin methods. *In preparation*, 2007.
4. S. Bertoluzza. Interior estimates for the wavelet galerkin method. *Numer. Math.*, 78:1–20, 1997.
5. F. Brezzi and M. Fortin. *Mixed and hybrid finite element methods*. Springer Series in Computational Mathematics, Vol. 15, Springer Verlag, New-York, 1991.

6. C. Canuto, A. Tabacco, and K. Urban. The wavelet element method. part i: Construction and analysis. *Appl. Comput. Harm.Anal.*, (6):1–52, 1999.
7. S. Chen, B. Merriman, S. Osher, and P. Smereka. A simple level set method for solving stefan problems. *J. of Comp. Phys.*, 135:8–29, 1997.
8. G. Chiavassa and J. Liandrat. On the effective construction of compactly supported wavelets satisfying homogeneous boundary conditions on the interval. *Appl. Comp. Harm. Anal.*, 4:62–73, 1997.
9. G. Chiavassa and J. Liandrat. A fully adaptive wavelet algorithm for parabolic partial differential equations. *App. Num. Math.*, 36:333–358, 2001.
10. C. Chui. *An Introduction to Wavelets*. Academic Press, 1992.
11. A. Cohen. *Wavelets Methods in Numerical Analysis*. in Handbook of Numerical Analysis, Editors P.G Ciarlet and J.L Lions, Elsevier Science Publishers, North Holland, 2000.
12. A. Cohen, I. Daubechies, and J.-C. Feauveau. Biorthogonal bases of compactly supported wavelets. *Comm. Pure. Appl. Math.*, 45(5):485–560, 1992.
13. I. Daubechies. *Ten lectures on wavelets*. SIAM, Philadelphia, 1992.
14. M. Elghaoui and R. Pasquetti. A spectral embedding method applied to the advection-diffusion equation. *J. of Comp. Phys.*, 125:464–476, 1996.
15. V. Girault and R. Glowinski. Error analysis of a fictitious domain method applied to a dirichlet problem. *Japan J. Indust. Appl. Math.*, 12, 1995.
16. J. Haslinger, J.F. Maitre, and L. Tomas. Fictitious domain methods with distributed lagrange multipliers. part 1: application to elliptic elliptic state problems. *Math. Models. Meth. Appl. Sci.*, 11:521–547, 2001.
17. A. Kunoth. Wavelet techniques for the fictitious domain-lagrange multiplier approach. *Numer. Algor.*, 27:291–316, 2001.
18. R. J. Leveque. *Finite volume methods for hyperbolic problems*. Cambridge Texts in Applied Mathematics, Cambridge University Press, 2002.
19. A.M Meirmanov. *The Stefan problem*. Walter de Gruyter, 1992.
20. Y. Meyer. *Ondelettes et Opérateurs I : Ondelettes*. Hermann, Paris, 1990.
21. M.Mommer. *Towards a fictitious domain method with optimally smooth solutions*. PhD thesis, RWTH Achen, 2005.
22. J.A Nitsche and A.H Schatz. Interior estimates for ritz-galerkin methods. *Math. Comp.*, 28:937–958, 1974.
23. R.H Nochetto, M. Paolini, and C. Verdi. An adaptive finite element method for the two phase Stefan problems in two space dimensions. part I stability and error estimates. *Math. Comp.*, 57:73–108, 1991.
24. R.H Nochetto, M. Paolini, and C. Verdi. An adaptive finite element method for the two phase stefan problems in two space dimensions. part ii implementation and numerical experiments. *SIAM J. Sci. Stat. Comp.*, 12, 1991.
25. S. Osher and J.A Sethian. Fronts propagating with curvature-dependent speed: Algorithms based on hamilton-jacobi formulations. *J. of Comp. Phys.*, 79:12–49, 1988.
26. V. Perrier and C. Basdevant. La décomposition en ondelettes périodiques, un outil pour l'analyse de champs inhomogénes. théorie et algorithmes. *la Recherche Aérospatiale*, 3:57–67, 1989.
27. A. Quarteroni and A. Valli. *Numerical approximation of partial differential equations*. Springer Series in Computational Mathematics, Vol. 23, Springer Verlag, New-York, 1997.
28. K. Schneider and M. Farge. Numerical simulation of the transient flow behaviour in tube bundles using a volume penalisation method. *Journal of Fluids and structures*, 20 (4):555–566, 2005.

29. J. Stefan. Uber die theorie der eisbildung. *Monatshefte Mat. Phys.*, pages 1:1–6, 1890.
30. J. Strain. Stability of planar solidification fronts. *Physica D*, 30:297, 1988.
31. R.F. Sekerka W.W Mullins. Stability of a planar interface during solidification of a dilute binary alloy. *J. Appl. Phys.*, 35:444, 1994.